Computational elastoplastic Limit Analysis of the Paderno d'Adda bridge (Italy, 1889)

Submitted for publication: July 6, 2016; Revised: March 17, 2017

Abstract

The Paderno d'Adda bridge is a historical iron arch bridge built in 1889 for connecting the provinces of Lecco and Bergamo across the Adda river, in northern Italy. The bridge was designed through the so-called *Theory of the Ellipse of Elasticity*. Its use is two-fold: a railway track lays within the inner deck of its upper continuous beam; automotive traffic runs on top. Today, after 128 years of continuous duty, the viaduct keeps in service, with trains crossing at slow speed and alternated one-way road traffic with no heavy-weight vehicles. Starting from a computational formulation for the elastoplastic Limit Analysis of 3D truss-frame systems, apt to provide the *exact* limit load multiplier and attached collapse mechanism, the full evolutive piece-wise-linear response of the bridge is derived, for different try-out loading configurations. The structural analysis, wholly original in its computational implementation, aims at outlining a survey on the potential plastic collapse characteristics of the bridge. Results reveal possible structural deficiencies for the upper continuous beam, where main plasticizations appeared; Instead, elements of the piers plasticized only for tests with loading much un-symmetrically located to the crown of the arch and the slender doubly built-in parabolic arch rarely showed any plasticization. This evidences the arch as a robust characteristic beautiful feature of the bridge. Moreover, analyses pointed out that the effect of the normal forces on the elastoplastic response of the bridge shall not considered to be negligible, as it may be often considered in the limit analysis of frames.

Keywords: *historical iron arch bridge; non-linear truss-frame FEM model; evolutive elastoplastic structural analysis; computational Limit Analysis; collapse load multiplier and mechanism.*

1 Introduction

In the present investigation, the evaluation of the global non-linear elastoplastic response of the historical iron arch bridge at Paderno d'Adda (northern Italy) is under target. This structure is a beautiful iron viaduct built in 1889 by the *Società Nazionale delle Officine di Savigliano (SNOS)* for the Board of Public Works of the Italian Government, in response to needs from rapidly-growing industrial activities in Lombardia towards the end of 19th Century (SNOS [1]). Specifically, within the expansion of the local railway network, it became necessary to acquire an elevated crossing on the river Adda, North-East from Milano, at about 85 m from water.

Designer Jules Röthlisberger (1851-1911), graduated at Polytechnic of Zürich in 1872, head of the SNOS Technical Office since 1885, elaborated a remarkable structural concept for the bridge. It was that of raising a stiff but slender symmetric doubly built-in parabolic arch among the two banks of Paderno d'Adda (right bank, province of Lecco) and Calusco d'Adda (left bank, province of Bergamo), of about 150 m of horizontal span and 37.5 m of vertical rise, supporting then, together with vertical truncated pyramidal piers, a straight upper box continuous beam on nine bearings of 266 m of length, with eight equal spans of 33.25 m (SNOS [1], Nascè et al. [2]) (Figure 1).

Figure 1: Contemporary upstream view of the Paderno d'Adda bridge (1889), from the Paderno d'Adda bank (right bank).

The bridge was designed through a practical application of the so-called *Theory of the Ellipse of Elasticity*, a graphical-analytical method of structural analysis that was developed in the wake of Graphic Statics, specifically at the Polytechnical School of Zürich by Karl Culmann (1821-1881) and his pupil Wilhelm Ritter (1847-1906). A specific account on that is provided in Ferrari et al. [3]. The bridge represents one of the very first large structures designed through such an elastic method of analysis and is considered now as a valuable repertory of industrial archaeology. The bridge was built by a wrought iron material, with riveted joints. According to the original SNOS Report (SNOS [1]), about 2600 tons of metals were employed in its construction. It was opened to traffic on May 1889, less than two years after the first start of the construction works (Nascè et al. [2]).

Nowadays, after 128 years of continuous duty, the viaduct keeps in service with trains crossing at slow speed and alternated one-way road traffic restricted to no heavy-weight vehicles. The structure appears rusted and most-likely set in a state of diffused and localized corrosion damage. Nascè et al. [2] argued that the state of deterioration of the bridge may be referring to a few design flaws and mainly to lack of maintenance. Along its history, the Paderno d'Adda bridge has undergone a few modifications and repairs. A restoration was carried out to repair damage caused by bombing during World War II. The whole roadway deck was replaced in 1972 by a steel orthotropic deck, connected by rivets to the original structure. Furthermore, in the early nineties, the replacement of some damaged structural members, the strengthening of the upper metallic box girder, a sand-blasting treatment and a very partial repainting were performed. Since that time, to the authors' knowledge, no other significant interventions on the bridge have been made.

As a matter of fact, the Paderno d'Adda bridge still plays a crucial role in the current lo-

cal transportation network and thus serious queries arise concerning its present and near future structural efficiency and destination.

In order to inspect first the original architectural and engineering conception of the bridge at design stage and the outcomes of the graphical-analytical design method adopted for the true calculation of the structure, a research project was started in 2005 at the University of Bergamo. The aims of that project were those to perform a complete modelling study on the bridge, to assess the present structural health conditions of the viaduct (Ferrari et al. [3–7]). This initially has led to the assembly of a complete linear FEM model of the structure, within a commercial FEM program, and then to the implementation of an independent non-linear model in a full elastoplastic framework, formulated autonomously within MATLAB. In particular, in Ferrari et al. [4], some of the original static loading configurations used for the design of the viaduct have been analysed, within the linear elastic range, as well as for the loading conditions that were implemented in the first try-outs in 1889. A comparison with the results from the original Technical Report by the SNOS (SNOS [1]) displayed a full consistency among reported data and present FEM post-predictions. Further, a first modelling investigation on the dynamic characteristics of the bridge has been attempted in Ferrari et al. [5], in terms of the determination of the main mode frequencies and associated mode shapes. The results from such a study appeared to be consistent to those from preliminary field investigations and dynamic identification on the bridge, based on ambient vibration tests that have been carried-out by colleagues at Politecnico di Milano (Gentile and Saisi [8]). This has further led to their development of a permanent Structural Health Monitoring system of the bridge (Gentile and Saisi [9]), as conceived to assess a possible degradation of the structural performance. Afterwards, the present research investigation on the bridge has been extended to the modeling of its global non-linear elastoplastic behaviour, as reported here. On this, preliminary elastoplastic analyses have been performed in Ferrari et al. [6][1]. In this context, a complete autonomous elastoplastic formulation and implementation for modeling general 3D truss-frame structures has been developed within the classical framework of the Theory of Plasticity and Limit Analysis (Ferrari et al. [7]).

The present research study is now moving on the direction of outlining a comprehensive modeling and interpretation of the global non-linear elastoplastic behaviour of the bridge, in this way representing, in fact, a first full advantage of the above mentioned computational code. In particular, the underlying FEM formulation and implementation introduced in Ferrari et al. [6, 7] is systematically involved and adapted to determine the collapse load multipliers and relevant collapse mechanisms of the structure, for various static try-out railway loading conditions made in 1889. In detail, the characteristic load/displacement curves are traced down by *exact* incremental analyses up to the true limit load and the critical members in the various parts of the structure are identified, specifically within the upper continuous beam. Analyses are also performed to evaluate different possible yielding responses of the structural truss-frame, in terms of axial force and bending internal actions, by considering two main cases of yield behaviour of the cross section (*Cases A* and *B*, as defined at the end of Section 2.2 and developed in the subsequent calculations and relevant comparison provided in Section 3.3). Moreover, by screening the plastic response of the structure up to collapse, interesting considerations are outlined by interpreting the geometrical configuration of the upper continuous beam of the bridge in terms of fundamental static schemes, as those of a double-cantilever or of a cantilever/simply-supported single span beam. Such considerations shall halp in understanding of the elastoplastic behavior of the bridge up to collapse, in the spirit of Limit Analysis.

Reference is made here so far to the characteristics of the bridge at design stage, as extracted from the original design technical drawings that are guarded at the *Archivio Nazionale di Torino*. Also, the hypothesis of perfect elastoplastic behaviour with unlimited ductility of all the structural members has been assumed, although by taking a reasonable conservative value of yield stress, according to the available original documentation (see SNOS [1], Nascè et al. [2]). The original computational features implemented in the solving algorithm allowed for tracking the complete limit structural behavior of the bridge, disregarding for the considerable number of dofs of the

[1] *Such preliminary analyses have been earlier presented at the SAHC12 Conference in Wroclaw, Poland.*

whole structural model, ranging in the order of thirteen thousands.

A brief account on the developed FEM formulation and on its code implementation is reported in Section 2; in the same section, specific computational aspects and additional considerations taken into account for the present elastoplastic analyses of the Paderno d'Adda bridge are provided as well. Section 3 illustrates the numerical results that have been achieved through the implemented algorithm, for the two considered yielding cases, and advances a critical analysis and interpretation. Section 4 presents global crucial considerations on the potential engineering implications of the present structural analyses, as concerning to the whole elastoplastic performance capacity of the viaduct. Summary comments on the study and a brief glance at future developments are finally pointed out in closing Section 5.

2 Non-linear elastoplastic 3D truss-frame FEM formulation

2.1 Framework of the computational algorithm

In the following, salient characteristic features of the non-linear elastoplastic FEM formulation implemented for the analysis of the Paderno d'Adda bridge are briefly resumed (for detailed information on the present computational implementation, one may refer to preceding companion work Ferrari et al. [7], and also to several pertinent references quoted therein, which were framing the present truss-frame implementation within the classical research context of structural Limit Analysis of frames).

Matrix notation is adopted throughout. Matrices and vectors are represented by bold-face characters. Transposition is indicated by superscript T. A dot marks a time rate, i.e. a derivative with respect to an ordering, not necessarily physical, time t.

The elastic FEM formulation is based on a classical Euler-Bernoulli beam finite element, according to the following peculiar hypotheses: straight element, uniform cross section, homogeneous material properties, transverse displacements modelled by cubic shape functions (i.e. negligible shear strain effects are considered), axial displacements and rotations varying linearly along the beam element. In the elastoplastic case, possible inelastic deformations may develop only at pre-selected sections (*plastic joints*). As a generalization of the classical plastic hinge concept in the Limit Analysis of frames, it is assumed that critical sections are located between adjacent conventional linear elastic finite elements.

The behaviour of the critical sections where plastic dissipation may be localized is described by an elastoplastic (perfectly-plastic) model with Piece-Wise-Linear (PWL) yield functions. This means that the relationships between static and kinematic generalized variables of the beam cross sections at the plastic joints are piece-wise linearized (see e.g. Maier [10, 11], Capurso [12], Hodge [13], Tin-Loi [14], Olsen [15]).

According to the idealizations above, following Eqs. (1)–(2) describe a general formulation of a PWL elastoplastic model in the critical section of a beam element:

$$\mathbf{q} = \mathbf{e} + \boldsymbol{\eta}, \quad \mathbf{e} = \mathbf{k}^{-1}\mathbf{N}, \quad \boldsymbol{\eta} = \mathbf{n}\boldsymbol{\lambda} \tag{1}$$

$$\boldsymbol{\varphi} = \mathbf{n}^T\mathbf{N} - \mathbf{Y} \leq \mathbf{0}, \quad \boldsymbol{\lambda} \geq \mathbf{0}, \quad \boldsymbol{\varphi}^T\boldsymbol{\lambda} = 0 \tag{2}$$

They relate generalized strain history variable $\mathbf{q}$ to generalized stress variable $\mathbf{N}$. In a usual 2D interpretation of truss-frames, for illustration purposes, the generalized strains in vector $\mathbf{q}$ consist of relative rotations at the extremities of the beam (with respect to a principal centroidal axis of the cross section) and of axial elongation (discontinuity of displacement along the centroidal axis of the beam); the generalized stresses gathered in vector $\mathbf{N}$ are the bending moments at the extremities of the beam and the axial force (Figure 2). This is then generalized to beam elements in 3D.

Eq. (1) splits strain variable vector $\mathbf{q}$ into an elastic addend $\mathbf{e}$ and a plastic (i.e. "irreversible") contribution $\boldsymbol{\eta}$ (Figure 2); the former is related to stress vector $\mathbf{N}$ through a positive-definite elastic stiffness matrix $\mathbf{k}$, and the latter to vector of plastic multipliers $\boldsymbol{\lambda}$ through matrix $\mathbf{n}$, the columns

Figure 2: Schematic description of a 2D beam finite element with plastic joints: (a) Static internal variables $\mathbf{N}$; (b) Kinematic plastic internal variables $\boldsymbol{\eta}$. This is then generalized to beam elements in 3D.

of which can be interpreted as $\mathbf{N}$-gradients of linear (or linearized) yield functions (associativity is assumed herein). In Eq. (2) yield functions are listed in vector $\boldsymbol{\varphi}$. Finally, constant vector $\mathbf{Y}$ collects the "yield limits" (for perfect plasticity), the *i-th* component of which represents the distance of the *i-th* yield plane ($i = 1, ..., y$) to the origin, in the space of generalized stresses $\mathbf{N}$.

Staying with a 2D idealization for the sake of description (in this work a full 3D formulation is developed), a linear rate relation can be obtained between the increments of: 6 static actions at the extremes of the beam element $\dot{\mathbf{H}}$, corresponding 6 nodal displacements and rotations $\dot{\mathbf{u}}$, above-mentioned 3 generalized kinematic plastic variables $\dot{\boldsymbol{\eta}}$. Namely (see Ferrari et al. [7]):

$$\dot{\mathbf{H}} = \mathbf{k}\dot{\mathbf{u}} + \mathbf{D}\dot{\boldsymbol{\eta}} \tag{3}$$

where $\mathbf{k}$ is the classical 6×6 elastic stiffness matrix of the finite element and $\mathbf{D}$ represents the 6×3 plastic stiffness matrix. Moreover, generalized stress vector $\mathbf{N}$ may be related to vector of static variables $\mathbf{H}$ (by equilibrium) as follows:

$$\mathbf{N} = \mathbf{Q}\mathbf{H} \tag{4}$$

where $\mathbf{N}$ is a 3×1 vector and $\mathbf{Q}$ is a 3×6 Boolean matrix.

When in a critical section some of the yield modes are active in the current time interval of the integration process, one has $\boldsymbol{\varphi} = \mathbf{0}$. In view of the incremental form of the governing equations, the rate form of the first relation in Eq. (2) and Eq. (4) is adopted:

$$\dot{\boldsymbol{\varphi}} = \mathbf{n}^T\dot{\mathbf{N}} = \mathbf{n}^T\mathbf{Q}\dot{\mathbf{H}} = \mathbf{0} \tag{5}$$

From a mathematical point of view, equality $\boldsymbol{\varphi} = \mathbf{0}$ represents a constraint equation (between the static internal variables) to be added to the "constitutive" relationship of the finite element, namely the relationship between vector $\mathbf{N}$ and vector $\boldsymbol{\eta}$.

In the solving procedure, a tangent stiffness formulation is adopted. This is achieved by the determination of an elastic-plastic matrix $\mathbf{k}_{ep}$ that renders a direct force/displacement (linear) incremental relationship. Through some straightforward mathematical steps, the following relation can be obtained for the generic beam finite element:

$$\dot{\mathbf{H}} = \mathbf{k}_{ep}\dot{\mathbf{u}} \tag{6}$$

Matrix $\mathbf{k}_{ep}$ is called "tangent stiffness matrix" and represents a direct force/displacement incremental relationship of a generic finite element when plastic deformation occurs, namely when stress point $\mathbf{N}$ in the space of the static variables keeps moving on a specific yield plane.

By assembling the tangent stiffness matrices of each finite element and the equivalent nodal force vector increment given by a specific loading configuration applied to the structure, the following global structural (linear) solving rate system is obtained:

$$\mathbf{K}_{ep}\dot{\mathbf{U}} = \dot{\mathbf{F}} \tag{7}$$

where $\mathbf{U}$ is the vector collecting the (un-constrained) degrees of freedom of the whole structure, $\mathbf{F}$ is the nodal force vector and $\mathbf{K}_{ep}$ is the global tangent stiffness matrix of the structure. Being this last rate relationship of a linear kind, the whole time integration process can be split into a sequence of time intervals in which all static and kinematic quantities vary linearly along each step.

2.1.1 Incremental procedure

The incremental procedure that can therefore be obtained for the solving elastoplastic algorithm is outlined as follows:

(i) At the beginning of the analysis, the structure is not under the effect of loading or of pre-existing stress states; then, no yield plane is active. Afterwards, the following quantity is set to be acting on the structure:

$$\mathbf{F}_{Li} = \lambda \mathbf{F} \tag{8}$$

where $\mathbf{F}_{Li}$ represents the incremental load, λ is a *load multiplier* and $\mathbf{F}$ represents the assembly of the equivalent nodal force vector coming from the given original load applied to the structure.

(ii) Thereafter, the formulation determines the incremental solution referred to above incremental load $\mathbf{F}_{Li}$, in terms of displacement increments. This solution is given by the structural (linear) solving system described in Eq. (7). The incremental solution in term of displacements $\Delta\mathbf{u}$ can be then computed. At the beginning of the analysis, stiffness matrix $\mathbf{K}$ is totally elastic, namely no yield plane is active at the structure's plastic joints.

(iii) From incremental solution $\Delta\mathbf{u}$, the corresponding increments of static internal variables can be determined, based on previous Eqs. (4) and (6):

$$\Delta\mathbf{N} = \mathbf{Q}\Delta\mathbf{H} = \mathbf{Q}\left(\mathbf{K}_{ep}\Delta\mathbf{u}\right) \tag{9}$$

Incremental solutions $\Delta\mathbf{u}$ and $\Delta\mathbf{N}$ do not take into account that some plastic modes may be possibly activated during the time step; on the other hand, it is possible that the extent of incremental load $\mathbf{F}_{Li}$ is not enough to determine the reaching of at least one internal static variable in a plastic joint on the corresponding yield limit. Through a comparison between each static internal variable at the beginning of the step and the corresponding yield limit, the algorithm calculates for each plastic mode, among all non-activated ones, the specific "scale factor" of multiplier λ leading to possible plastic activations.

(iv) So, the original incremental solution is rescaled proportionally, and the static and kinematic quantities of the structure at the end of the step are updated. At the end of the step some yield planes (at least one) are now activated. The stiffness matrix is therefore updated, becoming elastoplastic. Live load $\mathbf{F}_{Li}$ is re-set equal to $\lambda\mathbf{F}$ and procedures **(ii)**–**(iii)** are repeated.

At this point, the internal kinematic variables, active along the time interval, are selected according to the active yield planes at its beginning. If the computed incremental solution that can be extracted from Eq. (7) would imply a negative dissipation rate for any of the active modes (for instance, if a tensile yielding axial force acts on a beam and, instead, a length shortening would be obtained in the incremental solution), then the corresponding active mode is actually deactivated, the stiffness matrix is newly updated and the incremental solution is re-computed. On the other hand, when an active mode has been deactivated at the beginning of the time increment and the incremental solution would render an increment of the static action corresponding to that mode, producing thus a violation of the perfectly-plastic yield condition (for instance, an axial force becoming higher than the yield limit, at the end of the time increment), this would mean that such a mode shall be included among the active ones, from the beginning of the time interval; then, the stiffness matrix has to be updated before a new computation of the incremental solution.

Once all conditions of non-negative dissipation and perfectly-plastic yielding described above are fulfilled, the algorithm calculates again, among all non-activated modes, load multipliers $\Delta\lambda$ leading to new possible activations. Step **(iv)** is therefore repeated and in the end the analysis starts again with a new step.

The collapse of the structure is reached when the minimum eigenvalue of global (updated) matrix $\mathbf{K}_{ep}$ calculated within step **(ii)** vanishes (as evaluated by a ratio between the minimum and the maximum eigenvalue coming below a given numerical tolerance, in an order up to 10^{-15}) and the corresponding eigenvector leads to a positive incremental dissipation for each active mode. The analysis allows then to trace the true evolutive elastoplastic response of the whole truss-frame structure, in the spirit of Limit Analysis.

2.2 Specific implementation for the Paderno d'Adda bridge

Reference is made here so far to the characteristics of the bridge at design stage. Also, the hypothesis of perfect elastoplastic behavior with unlimited ductility of all the structural members is assumed, though by taking an assumed conservative value of the yield stress, as stated below.

According to the hypotheses stated in Section 2.1, in the elastoplastic analysis of the bridge it is assumed that the plastic deformations of the structure may occur only at pre-selected cross sections (plastic joints). In particular, potential plastic deformation is concentrated at the beam element edges, referred to as A and B, where two plastic joints are inserted. The assumed generalized kinematic variables in each plastic joint are consistently generalized to 3D elements, namely they become: two relative plastic rotations (each around a principal axis of the cross section - labels 1,2); a plastic axial elongation; a plastic relative rotation around the beam axis. Specifically, axial elongation and axial rotation are (possibly) activated in only one of the two joints (A or B), in order to avoid unrealistic rigid body movements; then, only 6 internal kinematic variables are required for each beam element. Shear effects have not been considered so far, considering the slender structural members of the bridge. In particular, a piece-wise-linear uncoupled behaviour is adopted for such internal static variables, namely a Rankine-type boxed-form yield domain in the space of the static variables is assumed.

The analytical description of the interaction domain for the beam finite element is then stated in terms of the following inequalities:

$$\begin{cases} N^- \leq min\left(N^{A,B}\right) \leq max\left(N^{A,B}\right) \leq N^+ \\ M_t^- \leq M_t \leq M_t^+ \\ M_1^- \leq M_1^{A,B} \leq M_1^+ \\ M_2^- \leq M_2^{A,B} \leq M_2^+ \end{cases} \tag{10}$$

where N is the axial force, M_t is the torque (uniform along the element), M_1 and M_2 are the bending moments with respect to the two principal axes of inertia of the cross section (indexes A and B referring again to the beam edges). Yield limits $N^-, N^+, M_t^-, M_t^+, M_{1,2}^-, M_{1,2}^+$ are assumed to be uniform along the beam and are obtained from material yield limits (σ_y, τ_y) and cross section geometrical characteristics as:

$$\begin{cases} N^+ = -N^- = A\sigma_y \\ M_{1,2}^+ = -M_{1,2}^- = \beta_f M_{1,2}^e = \beta_f \left(2J_{1,2}/h_{1,2}\right)\sigma_y \\ M_t = \beta_t M_t^e = \beta_t \left(J_t/b\right)\tau_y \end{cases} \tag{11}$$

where β_f and β_t are bending and torsion section shape factors (taken here as $\beta_f = 1.1$ and $\beta_t = 1.5$ for all the elements) and $J_{1,2}, J_t, h_{1,2}, b$ are flexural inertias, torsional inertia, heights and profile thickness of the cross section.

In the specific implementation for the Paderno d'Adda bridge, the data referred to each cross section of the structural members used to determine the quantities above have been exported, into the present MATLAB implementation, along with the morphological features of the bridge, from a previously developed linear FEM model, assembled within a commercial FEM code (Ferrari et al. [4,5]). It consists of a 3D truss-frame structure with beam elements, mutually connected at the nodes, obtained as an assembly of three main structural parts:

- bearing doubly built-in parabolic arch;
- vertical piers;
- upper box continuous beam.

The complete 3D truss-frame elastoplastic FEM model of the Paderno d'Adda bridge is represented in Figure 3; it collects 5337 beam elements, 2216 structural nodes and 13296 degrees of freedom (nodal displacements and rotations after assembling and before constraining) and is fully symmetric with respect to the vertical longitudinal plane of the viaduct.

To characterize such a model in terms of mechanical properties, some information about the material properties of the bridge have been acquired from SNOS [1] and Nascè et al. [2]. These refer to tests performed in 1955 and 1972, during the restoration of the bridge after World War II

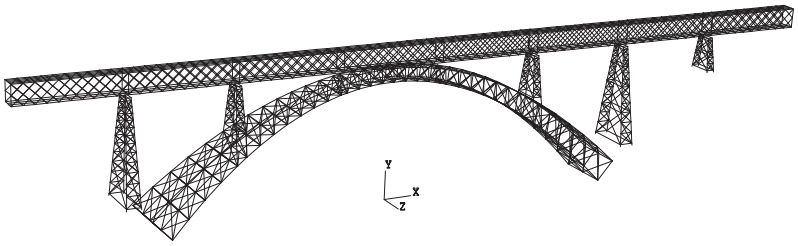

Figure 3: Assembled elastoplastic FEM model of the Paderno d'Adda bridge (1889).

and the replacement of its roadway deck, respectively. In particular, material tests were carried out on samples from the upper continuous girder, specifically from the diagonal elements of the wall beams and the transverse elements of the road support system (1955), and from some windbracing elements (1972). While in 1955 only tensile tests were carried-out, in 1972 chemical analyses, macro and micrographic examinations, resilience and bending tests were additionally performed. Results revealed rather poor metallurgical, chemical and mechanical characteristics. The yield stress obtained by the tests resulted generally larger than 240 MPa (minimum value equal to 227 MPa), with a tensile strength often less than 340 MPa and a rather low elongation (13% of average value, minimum value equal to 4%). According to the International classification of Philadelphia, 1876 (SNOS [1], Nascè et al. [2]), the bridge metallic material shall be classified as a "wrought iron".

Representative material properties of such a material have been thus adopted in the FEM model of the bridge, namely: Young's modulus $E = 17 \cdot 10^6$ t/m^2 $\simeq$ 170000 MPa; Poisson's ratio $\nu = 0.3$ (corresponding shear modulus $G = 6.54 \cdot 10^6$ t/m^2 $\simeq$ 65400 MPa); mass density $\rho = 7.7$ t/m^3 $\simeq$ 77 kN/m^3. Despite that the limit strength characteristics of the material could be set to those tipically reported for an iron material, considering also the limited ductility stated just above, the yield limits assumed in the present computational implementation have been then taken with reference to the design yield limits imposed by the SNOS at design stage (SNOS [1]): $\sigma_y = 6.00$ kg/mm^2 $\simeq$ 60 MPa, $\tau_y = \sigma_y/\sqrt{3} = 3.46$ kg/mm^2 $\simeq$ 34.6 MPa. These values characterize the previously introduced interaction domain for the beam finite element, adopted in the present computational implementation, leading to the evaluation of the elastoplastic structural response of the bridge up to collapse. In the present work, the limit analysis of the bridge has also been performed according to different assumptions for the definition of the interaction domain for the plastic joints of the beam finite element. This is explained below.

2.2.1 Considered two yielding cases

In the limit analysis of frames, bending actions generally play a dominant role with respect to axial and torsional actions, in the global elastoplastic response of the structure (Jiràsek and Bažant [16]). In some cases, it may be assumed that an unlimited yield limit for the axial force and the torsional internal static variables may be attributed to the cross section; namely, it may be stated that the space of generalized stresses is limited only by the yield planes related to the bending moments (if shear effects are not considered, as in the case treated herein).

For the present limit analysis of the Paderno d'Adda bridge, such a case has been also taken into account and treated in the forthcoming discussion. This has been additionally achieved by reducing the analytical description of the interaction domain for the beam finite element to just the last two inequalities in Eq. (10), related to bending moments $M_{1,2}$. Operationally, in the finite element formulation of such a case, the yield stress limits on the axial force and on the torsional moment have been set equal to one thousand times the corresponding values of the assumed yield stress limits on the bending moment. Under such an assumption, the structural response of the bridge up to collapse has then been re-evaluated.

Accordingly, in following Section 3, reporting the whole results of the performed elastoplastic limit analyses of the bridge, two main yielding cases have been considered:

- *Case A*. It indicates the reference yielding case considering the space of generalized stresses as

limited by the yield planes related to axial force, bending and torsional moments, according to the conservative yield stress values σ_y, τ_y stated above.

- *Case B*. It indicates a further yielding case considering the axial force and torsional internal static variables as associated to an almost unlimited yield stress (namely one thousand times the previous yield values, on the plastic axial force and on the torsional moment).

In practice, *Case A* represents the main reference case, as treated in the whole body of Section 3.1, while *Case B* is handled as a further special case, bringing in new information, as it is additionally presented in Section 3.2, and then discussed for comparison and interpretation in Section 3.3.

3 Limit analyses of the bridge

3.1 Loading configurations and numerical results

In this section, focus is made on the determination of the collapse load multipliers and relevant collapse mechanisms, for eight static try-out railway loading conditions that were performed on the bridge by the SNOS on 12–19 May 1889 (SNOS [1], Nascè et al. [2]). Tests (Figure 4) were carried-out using six locomotives with tender, each of 83 t $\simeq$ 830 kN of weight, corresponding to a uniformly-distributed load on the beam of about $q = 5.1$ t/m $\simeq$ 51 kN/m.

In the performed numerical simulations, such loading configurations have been imposed through vertical loads applied to the nodes of the FEM model of the bridge at the railway level. In Figure 4, total load Q applied to the structure is reported for each try-out test. Notice that Tests I–II and Tests V–VIII display three loaded spans, each of 33.25 m of length, for a total load of $Q = 509$ t, while Tests III–IV differ from the other ones in having only two loaded spans, for a total load of $Q = 339$ t. Self-weight is pre-loaded on the bridge (permanent load through specific weight ρ), leading to elastic deformations, before starting the incremental elastoplastic analyses, which then develop at increasing service load $P = \lambda Q$, as affected by linear load multiplier λ.

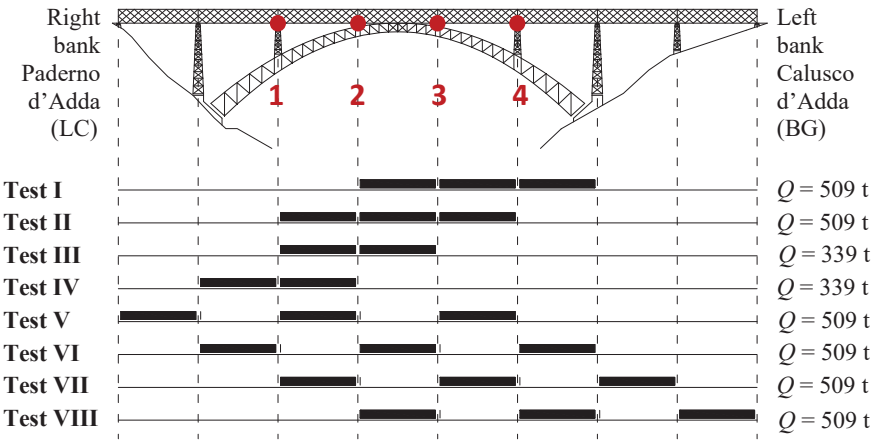

Figure 4: Scheme of eight considered static try-out (12–19 May 1889) configurations (view from downstream), with values of vertical total load Q applied to the structure for each test and indication of four Control Points 1–4 (red circles) at the beam/piers interfaces on the arch.

3.1.1 Main global results for reference *Case A*

Salient results of the elastoplastic analyses are presented first for reference *Case A* (see end of Section 2.2) in Figures 5–9 and Tables 1–2. All following representations of the elastoplastic bridge response up to collapse have been generated after running the limit analyses, by appropriate post-processing of the stored data.

For each of the eight considered try-out loading configurations (Figure 4), Figures 5-6 report on the left the deformed configuration of the bridge at incipient collapse (namely, the collapse mechanism) and a "plasticity map" of plastic activations in the various structural members, at increasing load multiplier λ, and on the right the characteristic non-linear load/displacement response curve (black curve), together with a second, complementary, representation of such a plasticity map.

In particular, the response curves on the right in Figures 5–6 have to be read on the lower and the left axes of each plot. The curves show the computed *exact* step-by-step evolutive solutions, with reference to values read at the beginning of each time interval. In particular, the lower horizontal axis depicts the vertical displacement (Δ) of the node that, in the end of the analysis, has displayed the maximum displacement at incipient collapse; the left vertical axis reports the amplified live load $P = \lambda Q$, where λ is the load multiplier related to the incremental solution of the non-linear elastoplastic analysis (Section 2.1). Notice that in these plots the non-zero initial displacement (at $P = 0$) is due to self-weight only, namely to a pre-imposed permanent load not affected by the load multiplier (i.e. load multiplier λ affects just the service load linked to the locomotive distributions). Moreover, for each loading case, the end point of the $P - \Delta$ curve refers to the so-estimated "exact" collapse of the structure in terms of vanishing minimum eigenvalue of the tangent stiffness matrix of the structure (Section 2.1).

In the same sketches reported on the right side in Figures 5–6, plasticity maps of plastic activations in the various structural members at increasing load multiplier λ are represented. These have to be read on the upper horizontal axis and on the right vertical axis, which depict the number of active modes and load multiplier λ, respectively. For each loading configuration, the map scores the plastic modes that are activated at the beginning of each time increment. Each marker represents one activated plastic mode in the structure, as described below. The activation of axial (N), bending (M) and torsional modes (M_t) are shown in green, red and blue, respectively. The type of marker refers instead to the part of the structure in which the activated plastic joint has appeared: to an element of the arch (diamond), piers (largest hollow circle), upper continuous beam (solid circle). So, in inspecting the plots, it is possible to appreciate the sequence of activation of the plastic joints, together with the overall plastic response of the bridge, at increasing load multiplier λ (and associated service load).

The sketches, are structured so as to read the response curves (black curves) and the plasticity maps, either on the left ($P = \lambda Q$) or on the right axis (λ), equivalently. Moreover, if a horizontal line is traced at some level of load, crossing the response curve at a particular point of interest, namely in correspondence of a particular step of the analysis, it is possible to inspect which kind of plastic modes and how many modes are active at that step, just by reading on the upper axis the intersection between such a horizontal line and the plasticity maps. Supplementary information about the activation of the plastic joints are also provided by the maps represented in the lower left part of each sub-figure, referred to each loading test, in which the sequence of activation of the plastic joints is emphasized.

Load multipliers λ_c at incipient structural collapse of the bridge for the eight loading configurations in Figure 4 are reported in Table 1, with the type and number of activated modes. Table 1 lists as well the maximum vertical node displacement of the bridge at incipient collapse (all maximum values actually refer to nodes of the upper continuous beam, at the railway level).

In the first four tests performed on the bridge (Figure 4), the highest values λ_c are obtained. Despite that in Tests I and II three spans of the upper continuous beam are interested by the service load distribution, in these tests the collapse load multiplier is not much different from those in Tests III and IV, where only two spans are loaded. As it can be appreciated in Table 1 and in Figures 5*a* and 5*d*, in Test I, near collapse, as in Test IV, many internal static variables in the elements of the piers reach yield planes referred to both bending moments and axial force. Moreover, Test IV presents the highest number of active modes in the piers (21 axial modes and 24 flexural modes). These modes are activated when the load multiplier reaches a value close to $\lambda = 3.2$ and seem then to rule collapse.

Screening the plasticized members depicted in red on the deformed configurations of the bridge at incipient collapse represented in Figures 5*a* and 5*d*, it is possible to note that, in Test I and in Test IV, all active modes in the piers arise in the elements placed on the arch, located towards the

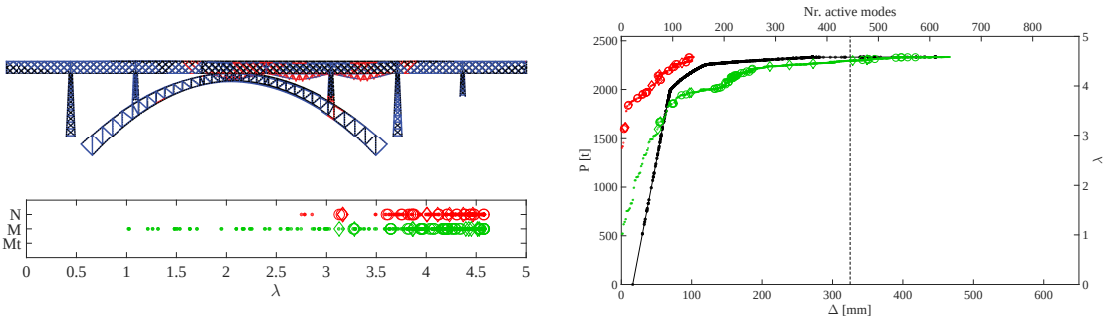

(a) Test I

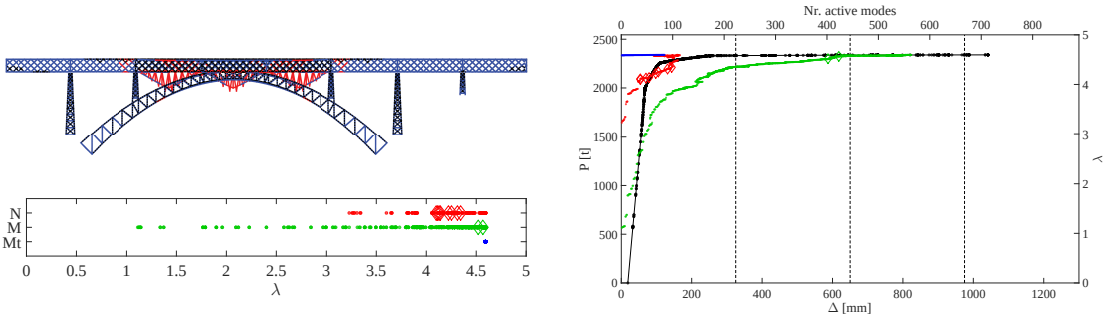

(b) Test II

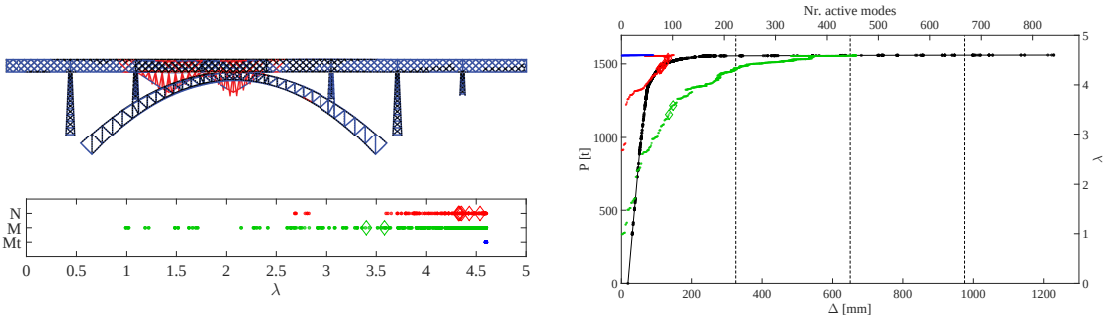

(c) Test III

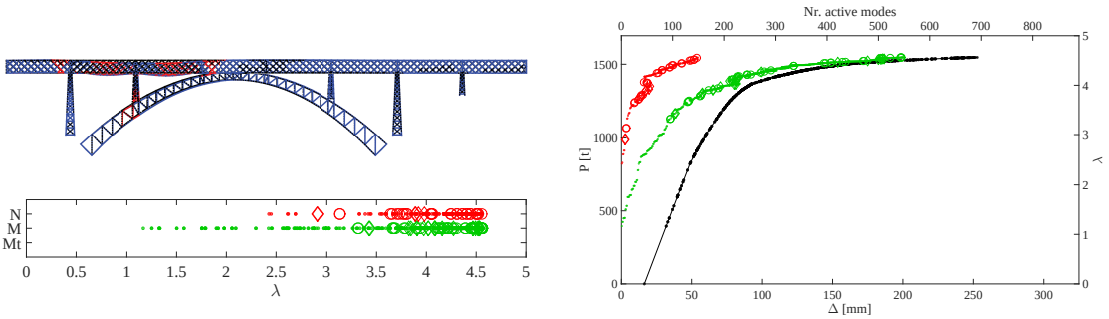

(d) Test IV

Figure 5: Representation of the elastoplastic deformed configurations (collapse mechanisms) of the Paderno d'Adda bridge at incipient collapse (amplification factor equal to 10) (top left), the plasticity maps (bottom left), and the characteristic load-displacement ($P - \Delta$) response curves together with plasticity maps (on the right), for the four loading configurations Test I–Test IV in Figure 4, *Case A*.

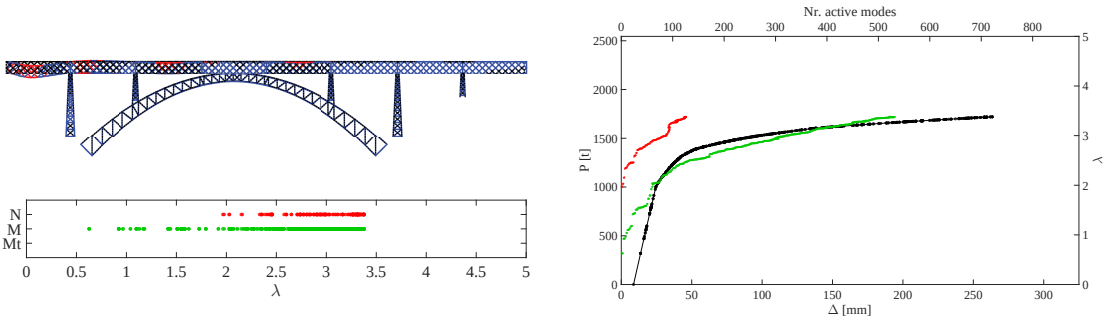

(a) Test V

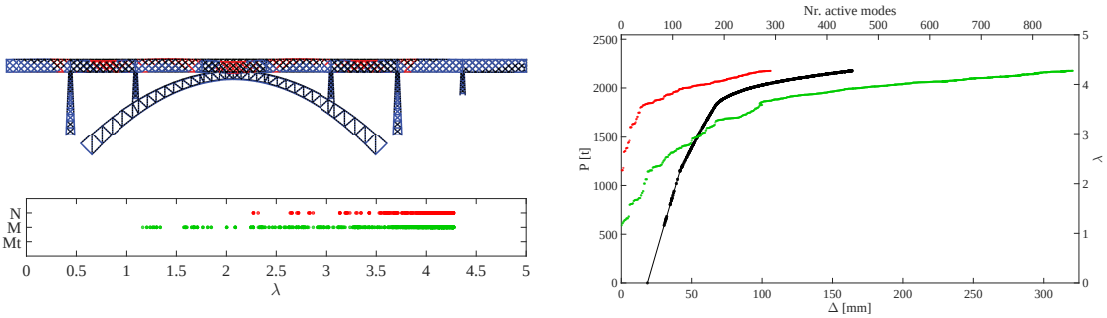

(b) Test VI

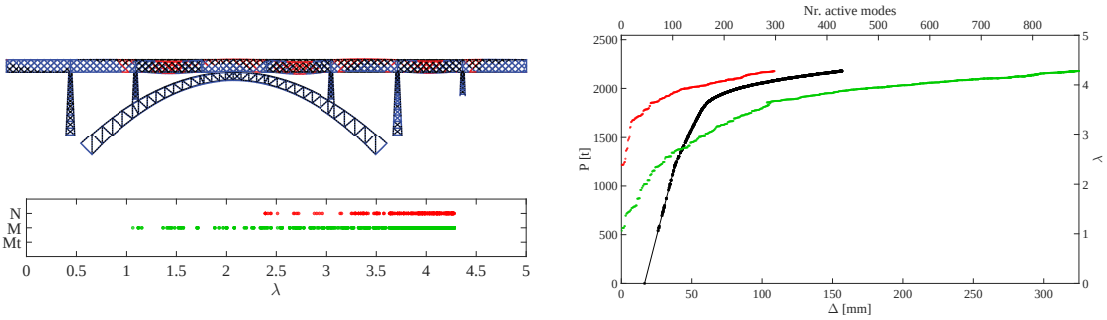

(c) Test VII

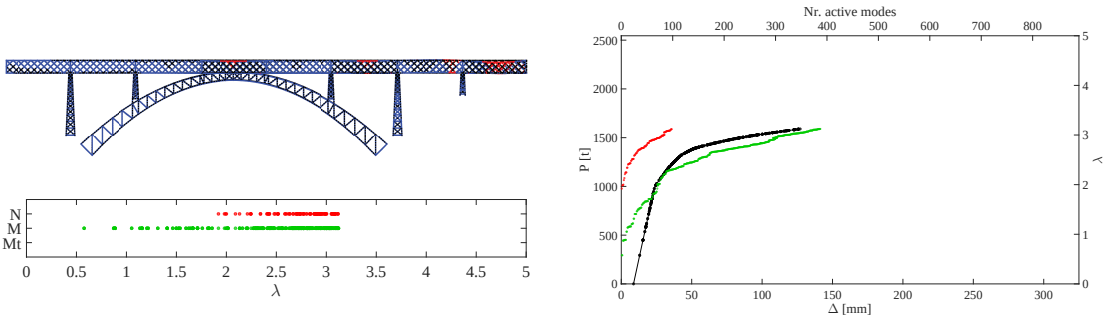

(d) Test VIII

Figure 6: Representation of the elastoplastic deformed configurations (collapse mechanisms) of the Paderno d'Adda bridge at incipient collapse (amplification factor equal to 10) (top left), the plasticity maps (bottom left), and the characteristic load-displacement ($P - \Delta$) response curves together with plasticity maps (on the right), for the four loading configurations Test V–Test VIII in Figure 4, *Case A*.

Table 1: Collapse load multiplier, active modes referred to Arch (A), Piers (P) and upper continuous Beam (B) and maximum vertical displacement of the bridge (beam nodes), *Case A*.

Test	Q [t]	λ_c	P_c [t]	**Nr. of active plastic modes**										Max vert.
				Axial				Flexural				Tors.	Tot	disp. [mm]
				A	P	B	Tot	A	P	B	Tot	B		
I	509	**4.59**	2336	8	16	115	139	9	12	613	634	0	773	447
II	509	**4.60**	2341	8	0	100	108	2	0	562	564	84	756	1042
III	339	**4.60**	1559	6	0	96	102	2	0	451	453	62	617	1228
IV	339	**4.56**	1546	6	21	122	149	20	24	503	547	0	696	253
V	509	**3.38**	1720	0	0	124	124	0	0	520	520	0	644	263
VI	509	**4.28**	2179	0	0	290	290	0	0	878	878	0	1168	164
VII	509	**4.28**	2179	0	0	296	296	0	0	893	893	0	1189	157
VIII	509	**3.12**	1588	0	0	98	98	0	0	387	387	0	485	127

Calusco bank and towards the Paderno bank, respectively. More in detail, Figure 7 shows that, in both Tests I and IV, the active modes refer to elements at the piers/arch connections and to elements of the upper rectangular closing frame on top of the piers, hosting as well the bearing devices of the beam. Some active modes arise also in the elements of the four faces of the box profile of the piers; in particular, in the elements of the front ones (laying in the same inclined planes of the arch profile).

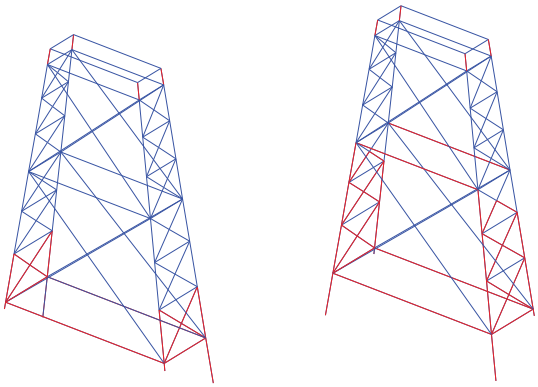

(a) ***(b)***

Figure 7: Representation of the activated members (in red) at incipient collapse of the pier towards the Calusco bank, Test I (a) and of the pier towards the Paderno bank, Test IV (b), *Case A*.

The plasticity maps in Figures 5*b* and 5*c*, for Test II and Test III, respectively, show that almost all yield modes activated at increasing load refer to the elements of the upper continuous beam; only very few plastic modes are activated in the elements of the arch and no yield modes appear in the piers. Moreover, torsional modes are activated close to value λ_c (in a number equal to 84 and 62 for Test II and Test III, respectively), seeming to rule collapse. The response curves obtained by the analysis referred to both Test II and Test III (Figure 5*b* and 5*c*) show significant plastic resources in terms of global structural ductility. In fact, at incipient collapse, these loading configurations lead to a prolonged plateau and to the highest maximum vertical displacement (Table 1), up to about four times the maximum displacement in the other tests, which is referred to nodes of the lower frame connecting the two main vertical longitudinal truss girders of the upper continuous beam, right underneath the rails, where the distributed load has been applied.

In Test V and Test VIII, the lower values of λ_c are obtained. These two tests are characterized by having loaded the spans at one end of the upper continuous beam. In Figure 6*a*, 6*d* and, in detail, in subsequent Figure 8 it is possible to appreciate the deformed configurations of the bridge at incipient collapse at the extreme spans referred to these two tests: many members of the first

and of the last span, with reference to Test V and Test VIII respectively, are activated (in red). No plastic modes are activated in the elements of arch and piers. Moreover, the maximum vertical displacements obtained In Test VIII at incipient collapse is, by far, the lowest. This is likely due to the different structural behavior that occurs when a span adjacent to the bank bearing is loaded, due to the simply-supported condition (free rotation) at one extreme of the span. In fact, if the same total load of Test V and Test VIII is considered (in terms of resultant Q), but distributed further away from the banks of the upper beam, the obtained collapse load multiplier increases.

(a) *(b)*

Figure 8: Particular of activated members (in red) at incipient plastic collapse of the upper beam's span adjacent to the Paderno bank, Test V (a) and of the upper beam's span adjacent to the Calusco bank, Test VIII (b), *Case A*.

It is worth to note that in the finite element modeling of the upper continuous beam, the boundary conditions corresponding to what was designed by the SNOS have been considered. Relative rollers with single free translation along the longitudinal axis of the bridge are imposed between the upper truss beam and the piers or bearings on the arch, except for the bearing at half length, where a relative hinge is imposed. Similar absolute rollers are imposed at the nodes at the extremities of the beam on the river banks, both on the bottom, at the level of the railway deck, and on the top, at the road deck. Under these assumptions, the spans located at the extremities of the upper beam do not fully profit of the continuity of the beam. In the presence of different boundary conditions, e.g. built-in constraints, it would be possible instead to take further benefit from such a continuity. In light of this, the results referred to Test V and Test VIII look linked to the design-stage characteristics of the upper beam. Specific investigations could be further conducted to query the real boundary conditions at the beam/banks connections and their possible implications on the resulting structural behaviour of the beam at its ends.

Similarly to Test V and Test VIII, Test VI and Test VII (Figures 6*b* and 6*c*) still show activated modes only in the elements of the upper continuous beam and that the number of them is the largest, exceeding one thousand (Table 1). However, the displacements obtained at incipient collapse remain lower than those referred to the first five tests of the bridge, showing, together with the case of Test VIII, quite limited plastic displacements.

Looking in detail at the deformed configurations depicted in Figures 5–6, it is possible to observe that they look quite similar to each other. In particular, deformations appear to be localized in correspondence of the railway level of the upper continuous beam (where the "active" load is applied), as it is better discernible in Figures 5*b* and 5*c*.

Actually, in all try-out tests only very few elements of the arch yield. Instead, the elements of the upper continuous beam appear to be the most critical ones in terms of plastic collapse.

3.1.2 Further control-point results for reference *Case A*

In order to investigate the global behavior of the bridge in more detail, further screenings of the results of the elastoplastic analyses have been produced. These are reported in Figure 9 and Table 2, still for *Case A*, as defined at the end of Section 2.2.

Figure 9 shows, for each test, the characteristic non-linear load/displacement response ($P-\Delta$) curves as read at the four control points (*CPs* 1–4) represented in Figure 4. These are localized at the pier/beam and arch/beam interfaces, at the railway frame level, and refer to the four bearings of the beam resting on the arch. In the figure it is possible to note that, at the selected *CPs*, the collapse of the bridge is generally reached without significant plastic deformation at this level. Only in Tests I and IV (Figures 9*a* and 9*d*), where the loads are much un-symmetrically located with respect to the crown of the arch, plastic displacements are visible at *CPs* 4 and 1,

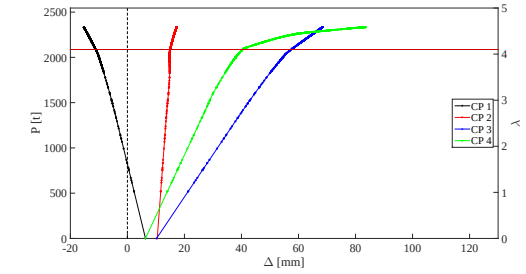

(a) Test I

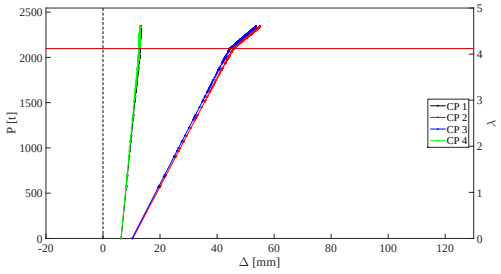

(b) Test II

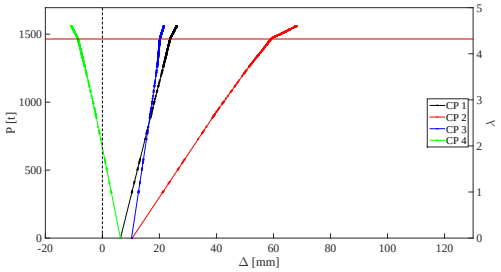

(c) Test III

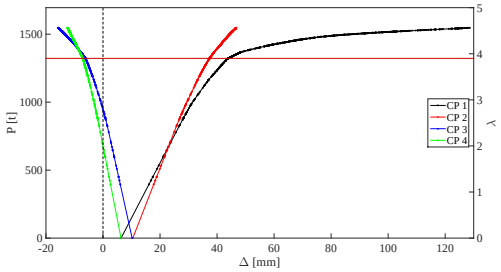

(d) Test IV

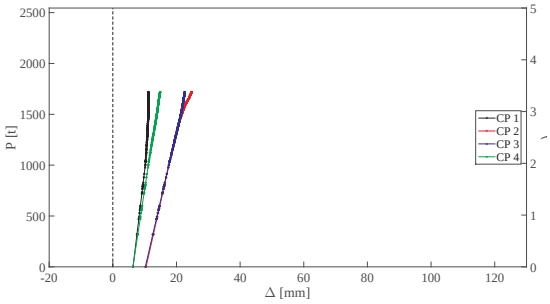

(e) Test V

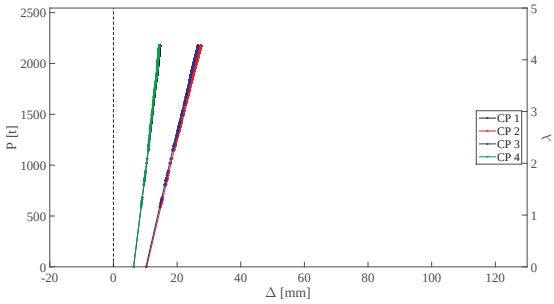

(f) Test VI

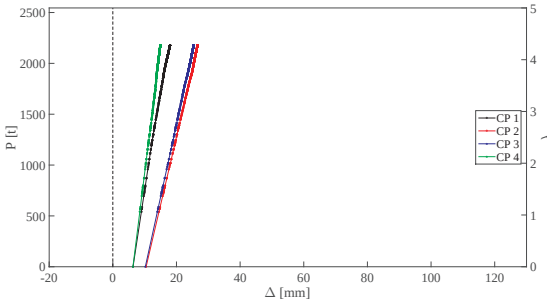

(g) Test VII

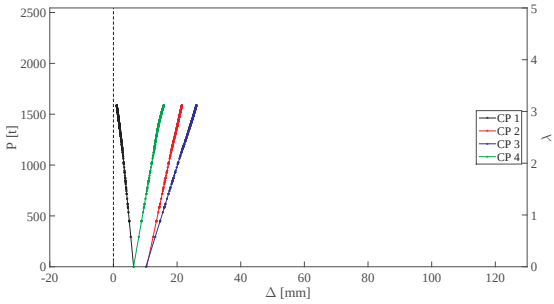

(h) Test VIII

Figure 9: Characteristic $P - \Delta$ curves at Control Points 1–4 in Figure 4, *Case A*.

respectively. In Test II, Test III and Tests V–VIII the characteristic $P-\Delta$ curves stop quite early: structural collapse of the bridge at the upper beam level is achieved without appreciable vertical displacement at the *CPs*. In Figures 9*a–d* the $P-\Delta$ curves abandon the linear elastic trend at total load $P_e = \lambda_e Q$ (marked by a red horizontal line). This load level marks a threshold beyond which further loading generates permanent plastic deformation as recorded at the *CPs* (λ_e in the order of $\lambda_e = 4.0$–4.1 for Tests I and II, $\lambda_e = 4.3$ for Test III, $\lambda_e = 3.9$ for Test IV). The $P-\Delta$ trends are almost linear, so that these response curves at *CPs* 1–4 display an almost bi-linear trend, with a visible kink at the level of the threshold line. The further post-kink load gain is quite limited, with respect to the threshold load. In Figures 9*e–h* the $P-\Delta$ curves show that the collapse of the structure is reached without plastic deformation as screened at the level of the selected *CPs*. From Figure 9 it is also possible to note that the maximum displacements manifested at the level of the *CPs* at incipient collapse are much smaller than those occurred at the railway level of the upper continuous beam (Figures 5–6). This is reflected in limited deformations of the piers on the arch and of the arch itself at incipient collapse.

The analyses seem to show that, for the considered loading configurations (Figure 4), the arch looks always quite far from plastic collapse. This assumption appears to be supported also by the results reported in Table 2 that lists, for each test, the values of the axial forces in the bars and the relevant normal stresses at the extrados and intrados of the arch shoulders. Stresses are all below the assumed target admissible values. Moreover, the stresses linked to the minimum and maximum axial forces in the various bridge elements, always appearing in the arch, are as well below target (last two columns in Table 2).

Table 2: Bridge FEM axial forces N [t] and stresses σ [kg/mm^2] at the arch shoulders and min/max values (always in the arch), for the test distributions shown in Figure 4, *Case A*. Negative values indicate compression.

N [t]	**Calusco shoulder**		**Paderno shoulder**		**Bridge element (arch)**	
σ [kg/mm^2]	Extrados	Intrados	Intrados	Extrados	Min	Max
Test I	-845458	-358977	119798	-1394470	-1394470	243844
	-5.29	-1.47	0.75	-5.72	-5.72	4.75
Test II	-421110	-1020350	-424148	-1017090	-1020350	244708
	-2.63	-4.18	-2.65	-4.17	-4.18	5.56
Test III	-34834.4	-1174700	-738870	-417237	-1177470	248489
	-0.22	-4.83	-4.62	-1.71	-4.83	5.64
Test IV	267882	-1138610	-624997	-177249	-1138610	267882
	1.68	-4.67	-3.91	-0.73	-4.67	1.68
Test V	-179807	-676097	-137289	-722763	-722763	102764
	-1.12	-2.77	-0.86	-2.96	-2.96	1.99
Test VI	-195880	-812012	-202086	-805328	-812012	125371
	-1.23	-3.33	-1.26	-3.30	-3.33	2.85
Test VII	-152484	-868321	-200817	-815524	-868321	133916
	-0.95	-3.56	-1.26	-3.34	-3.56	2.59
Test VIII	-328300	-464883	-75079.9	-740941	-740941	119461
	-2.05	-1.91	-0.47	-3.04	-3.04	2.71

3.1.3 Interpretation of results for reference *Case A*

Further, elastoplastic results reported in Table 1 and Figures 5–6 lead to outline two main important considerations for the interpretation of the recorded limit analysis elastoplastic response of the bridge:

(a) The collapse load multipliers among Tests I–IV, VI–VII and among Tests V and VIII are separately rather homogeneous, disregarding for the loaded spans (Figure 4). This seems to suggest that the adoption of a FEM modelization with a single loaded bridge span should lead to similar collapse load multipliers.

(b) Differences between the collapse load multipliers for Tests I–IV, VI–VII vs. for Tests V and VIII outline a possible connection between the schemes of a double cantilever beam, for the former, and of a cantilever/simply-supported beam, for the latter, as extremity conditions for the upper continuous beam.

According to such path of reasoning, the following confrontation is made:

(1) The collapse load multipliers of a single span resting on firm vertical supports were calculated by the FEM modelization with the same elastoplastic algorithm, giving rise to results sketched in Figure 10. Therein, value $\lambda_c^{in} = 4.60$ for the collapse of an inner span, referring to a double cantilever condition, may be compared to the average of the collapse load multipliers λ_c for Tests I–IV, VI–VII, namely $\overline{\lambda}_c^{\bullet} = 4.485$, and value $\lambda_c^{ex} = 3.54$ for the collapse of an external span, referring to a cantilever/simply-supported condition, may be compared to the average of the collapse load multipliers λ_c for Tests V and VIII, namely $\overline{\lambda}_c^{\circ} = 3.25$. This is already an astonishing matching. Moreover, it is worth noting that single span FEM value λ_c^{in} exactly corresponds to collapse load multipliers λ_c referring to Tests II and III. Also, $\lambda_c^{in} = 4.60$ is larger than $\overline{\lambda}_c^{\bullet} = 4.485$ and $\lambda_c^{ex} = 3.54$ is larger than $\overline{\lambda}_c^{\circ} = 3.25$, as it may be expected, given the firm supports and strict cantilever conditions on the single span FEM modelizations.

(2) The collapse load multipliers from classical Limit Analysis of either a double cantilever or a cantilever/simply-supported single span beam under uniform load, as sketched in Figure 11, may be compared to the load multipliers of the whole bridge FEM model from Table 1. This comparison points out a confrontation between ratios of $\lambda_c^{\bullet}/\lambda_c^{\circ} = 16/11.65 = 1.37$, for classical Limit Analysis results on a beam, vs. $\overline{\lambda}_c^{\bullet}/\overline{\lambda}_c^{\circ} = 4.485/3.25 = 1.38$. This constitutes as well a further astonishing matching. Moreover, collapse load multiplier ratio $\lambda_c^{in}/\lambda_c^{ex} = 1.30$ in Figure 10 is also rather homogeneous with ratio $\lambda_c^{\bullet}/\lambda_c^{\circ} = 1.37$ in Figure 11.

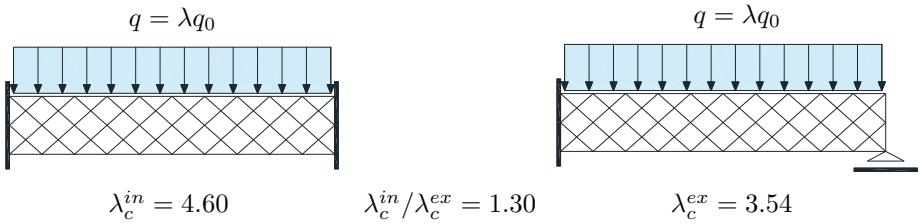

Figure 10: Collapse load multipliers obtained by the FEM modelization of a single span of the Paderno d'Adda bridge under uniform live load. Collapse load multiplier λ_c^{in} refers to the inner spans of the bridge, like in a double cantilever condition (left); collapse load multiplier λ_c^{in} refers to the external spans of the bridge, like in a cantilever/simply-supported condition (right).

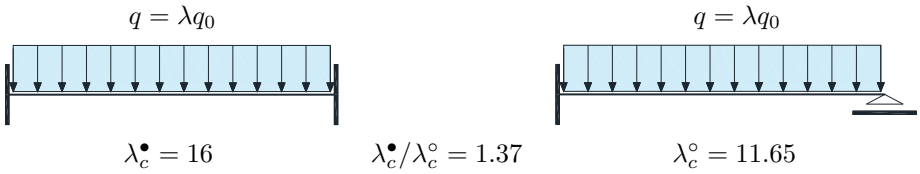

Figure 11: Collapse load multipliers obtained from classical Limit Analysis of a double cantilever (left) and of a cantilever/simply-supported (right) beam under uniform live load.

3.2 Limit analysis of the bridge with yield domain limited only on bending moments (*Case B*)

Further obtained results related to *Case B*, as explained in Section 2.2, are discussed in what follows and reported in Figures 12–13 and Table 3. This case considers an (almost) unlimited

yield domain in terms of axial force (and torsional moment) in view of the following two main motivations:

(i) Such a hypothesis is often adopted in the limit analysis of frames, where main plastic influence is attributed to the bending moment effects; it looks then interesting to compare previous results, accounting also for axial force (and torsional moment) plastic contributions, in view of interpretation of the outcomes of such a typical assumption, within the present context of tracing a complete evolutive elastoplastic response of truss-frame structures.

(ii) Privileging the role of bending moments in the yielding response, with respect specifically to axial force, may display relevant implications in terms of the wanted strengthening effect that was implemented by the windbracing systems in the true three-dimensional box truss-frame macro-structural elements of the bridge, in terms of constrained axial elongation of the various members; this may induce visible effects, possibly to be recorded for the considered try-out loading conditions, concerning collapse load multiplier and attached collapse mode, then helping in the whole interpretation of the elastoplastic response of the bridge, also in line of just achieved results and comments as already outlined in Section 3.1.3.

Screening the plastic response curves of the bridge at increasing load multiplier (black curves in the right sketches of Figures 12–13), it is possible to observe that the global response of the bridge for *Case B* does not differ substantially among the eight considered loading cases (Figure 4). As a main characteristic outcome, the values of collapse load multiplier λ_c appear set at around a similar value, nearly equal to $\lambda_c \simeq 4.5$ (see Table 3), regardless for the amount of total load Q applied to the bridge structure.

In other words, the strengthening effect implemented by an (almost) unlimited yield boundary on the axial force leads to a visible *levelling* of the collapse load multipliers for the different loading conditions. This could be further appreciated in Figure 14, as shown and discussed below.

Collapse load multipliers for Tests V and VIII are even much related now (actually equal) and become closer to the other ones, which are homogeneous whithin themselves (Table 3, Figure 14). Thus, within the achieved strengthening effect, the implications of the different rotation-free boundary condition of the extreme spans of the beam do not have that kind of influence and results look much homologous to those of a single double cantilever loaded span (as discussed earlier in Section 3.1.3).

In Tests III and IV, where only two spans are loaded, a main difference with respect to the other configurations refers to the fact that only the maximum displacement showed by the bridge at incipient collapse differs, which is equal to about two times and four times the maximum displacement referred to the other cases, for Test III and Test IV, respectively.

In the analyzed loading tests, plastic activations result largely localized in the upper continuous beam. Plastic joints in the piers are activated only in Tests I and IV, equal in number to 24; only two plastic joints appear instead in the arch, in Tests I and III. These activations are likely associated with the configuration of the loads applied to the bridge as referred to Tests I–IV, which entails, compared to the other loading configurations (Tests V–VIII), higher reaction forces at the interfaces between the upper beam and the underlying piers and arch. Observing the characteristic non-linear load/displacement response curves in Figures 12–13, it is possible to note the presence of clear "kinks" in the trends of the curves. In Tests I and II this presence is very visible. In particular, two kinks mark the transition between the initial linear elastic trend of the curves and the final horizontal plateau. In Tests III and IV this phenomenon is less prominent, meanwhile in Tests V–VIII only one kink appears, at the end of the linear elastic trend of the curves. By inspecting the plots, it is also possible to note that such kinks usually manifest themselves when a substantial increase in the number of plasticizations occurs in correspondence of an almost constant value of the load multiplier. In the right sketches of Figures 12–13, this phenomenon is highlighted by a plateau of the represented plasticity maps.

Regarding the deformed configurations, comments stated for *Case A* may also relate to this case.

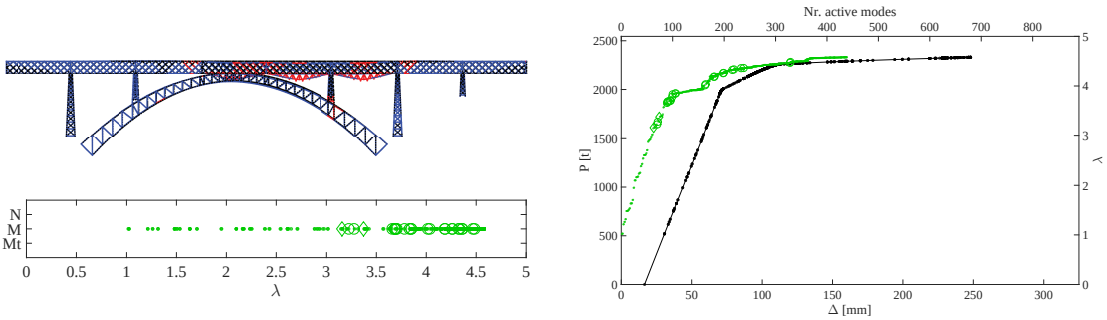

(a) Test I

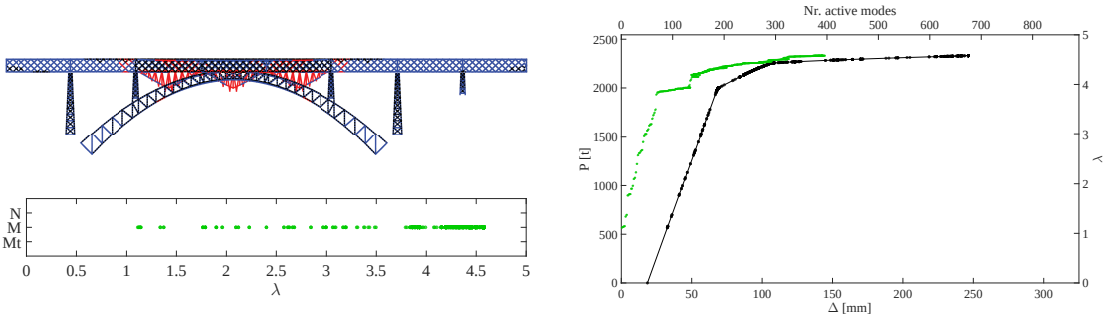

(b) Test II

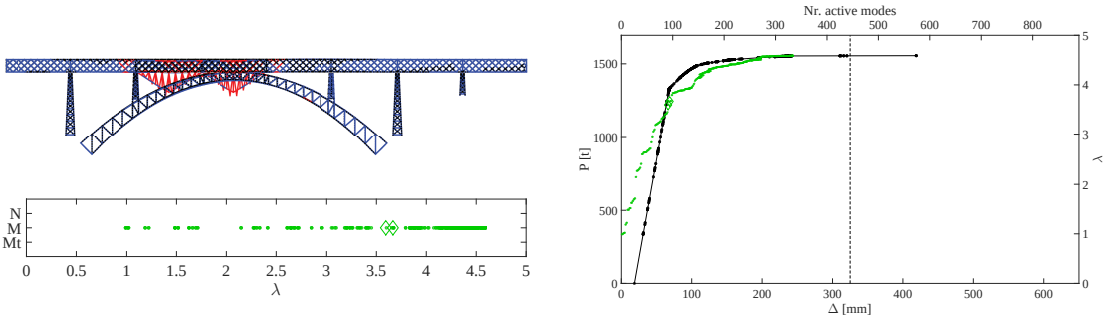

(c) Test III

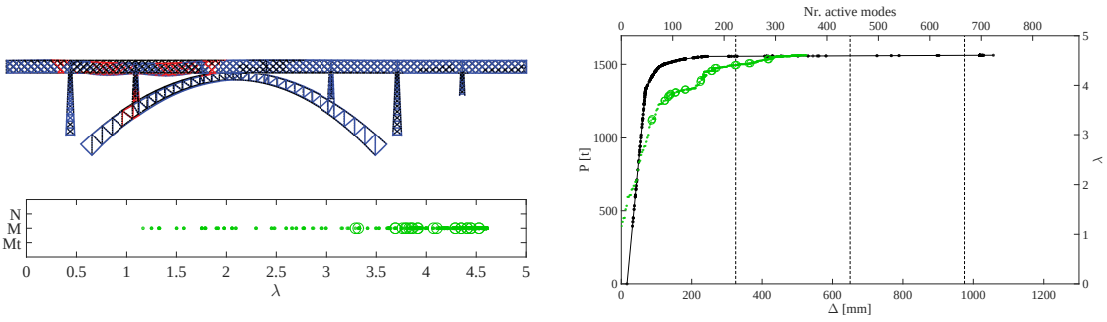

(d) Test IV

Figure 12: Representation of the elastoplastic deformed configurations (collapse mechanisms) of the Paderno d'Adda bridge at incipient collapse (amplification factor equal to 10) (top left), the plasticity maps (bottom left), and the characteristic load-displacement ($P - \Delta$) response curves together with plasticity maps (on the right), for the four loading configurations Test I–Test IV in Figure 4, *Case B*.

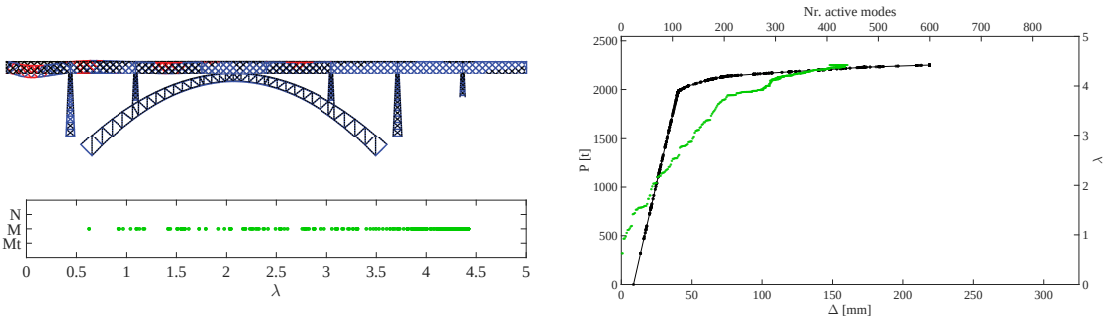

(a) Test V

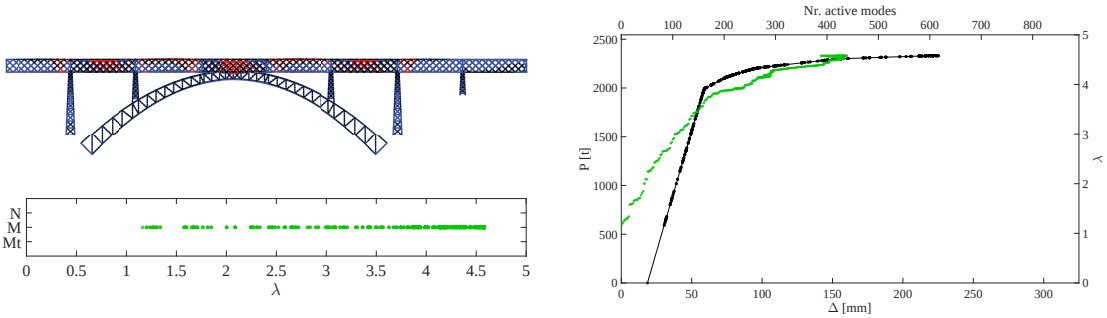

(b) Test VI

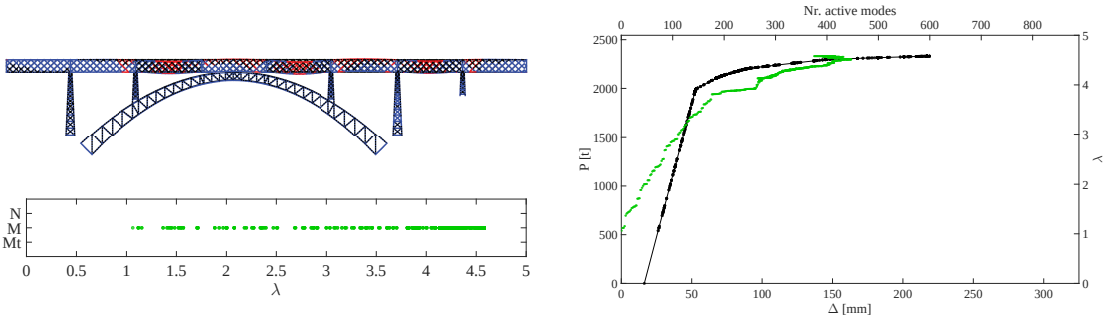

(c) Test VII

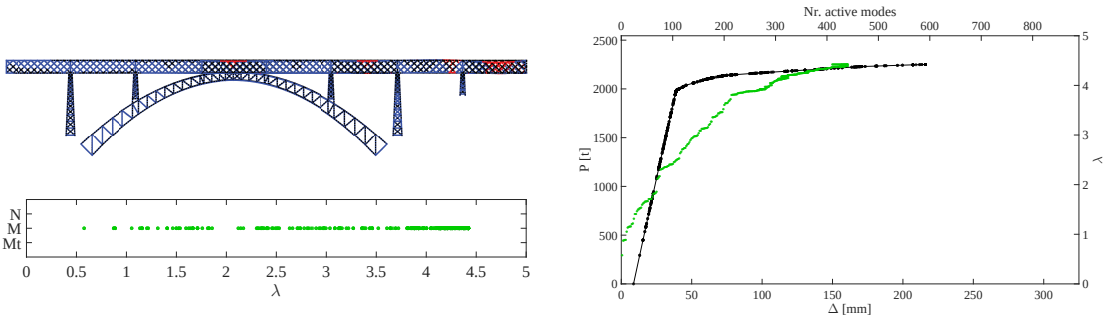

(d) Test VIII

Figure 13: Representation of the elastoplastic deformed configurations (collapse mechanisms) of the Paderno d'Adda bridge at incipient collapse (amplification factor equal to 10) (top left), the plasticity maps (bottom left), and the characteristic load-displacement ($P - \Delta$) response curves together with plasticity maps (on the right), for the four loading configurations Test V–Test VIII in Figure 4, *Case B*.

Table 3: Collapse load multiplier, active modes referred to Arch (A), Piers (P) and upper continuous Beam (B) and maximum vertical displacement of the bridge (beam nodes), *Case B*.

Test	$Q[t]$	λ_c	$P[t]$	**Nr. of active plastic modes** Flexural modes			Total	Max vert. disp. [mm]
				A	P	B		
I	509	**4.58**	2331	2	24	411	437	248
II	509	**4.58**	2331	0	0	391	391	247
III	339	**4.59**	1556	2	0	332	334	419
IV	339	**4.61**	1563	0	24	335	359	1057
V	509	**4.42**	2250	0	0	434	434	219
VI	509	**4.58**	2331	0	0	439	439	225
VII	509	**4.58**	2331	0	0	416	416	219
VIII	509	**4.42**	2250	0	0	441	441	216

3.3 Comparison among *Cases A* and *B* and interpretation

Interesting considerations may be finally stated by comparing the main results earlier obtained for reference *Case A* (Figures 5–7 and Tables 1–2) to the additional ones related to *Case B* (Figures 12–13 and Table 3). Towards this specific end, following Figures 14–15 have been additionally generated.

In Figure 14, white edged squares and blue circles schematically show the value of the collapse load multipliers referring to *Case A* and to *Case B*, respectively. The number of the plasticized members at incipient collapse is depicted as well in Figure 15, through bar plots. Dark blue and light blue bars refer to *Case A* (in particular to axial modes and bending modes, respectively), magenta bars refer to *Case B* (only bending modes).

From the obtained results it is possible to note that for Tests I–IV the collapse load multipliers related to the two analyzed cases do not change significantly. Indeed, in these loading configurations the number of plasticized members of the bridge at incipient collapse for *Case B* appears lower than the number of the activated modes related to *Case A* (Figure 15). For Tests VI and VII the load multiplier appears slightly minor for *Case A*. A significant increment of load multiplier has instead been obtained for Tests V and VIII (increment around 40%). Only in Test VIII the structure reaches collapse by showing a larger number of plasticized members for *Case B* than for the number of plasticizations related to *Case A*, with reference to bending modes only (in a number of 387 (*Case A*) vs. 411 (*Case B*)).

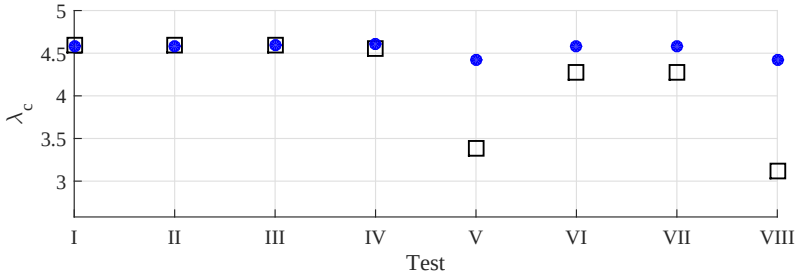

Figure 14: Representation of values of collapse load multiplier λ_c for *Case A* (white squares) and *Case B* (blue circles), for each loading test performed on the bridge (Figure 4).

The larger increase of the collapse load multiplier that has been obtained refers to the tests for which the load weights on the spans near the bearing banks (Figure 4, Test V and Test VIII). As stated earlier, these loading configurations, for *Case A*, have turned out to be the most restrictive ones in terms of global ductility revealed by the structure. This means that, for such configurations, the plastic structural response of the bridge is influenced by the strengthening effect due to the locked axial elongations. In fact, by increasing the yield limit related to the axial force, the collapse

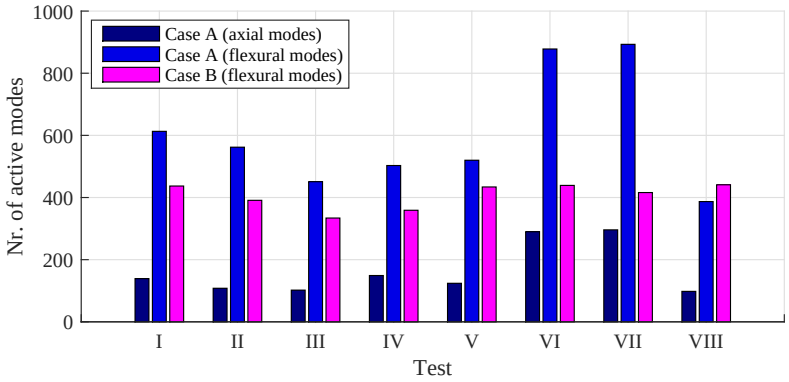

Figure 15: Bar plot representing the number of axial and flexural modes activated at incipient elastoplastic collapse for each loading test performed on the bridge (Figure 4). Dark and light blue bars refer to *Case A*; magenta bars refer to *Case B*.

load multiplier increases and leads to the levelling effect as commented above, with a characteristic collapse value at around $\lambda_c = 4.50$ for all the considered loading cases.

Incidentally, the strengthening effect on the upper deck of the continuous beam that has been implemented in the orthotropic deck restoration in 1972 and in the later strengthening of the metallic box girder (Section 2.2) looks likely consistent with the outcomes displayed by the FEM elastoplastic simulations for *Case B*. In this sense:

(i) hypothesis of *Case B* may look much consistent for the present modelling of the actual morphology of the deck and relevant achieved strengthening effect, with respect to the original configuration at design stage;

(ii) the restoration intervention shall have indeed stiffened the upper continuous beam, then by displaying as a documented effect from the present analyses, a higher resilience that should be displayed by the structure in terms of elastoplastic collapse. In practice, the structural interventions shall have indeed consolidated the bridge macro-element (upper continuous beam), which looks as the weaker macro-element of the bridge in terms of global plastic collapse, according to the present limit analyses.

4 Global remarks on the structural elastoplastic analyses

Under the fundamental assumption of referring to the morphological and mechanical characteristics of the bridge at design stage, the following main itemized considerations emerge out of the performed evolutive elastoplastic analyses on the bridge up to structural plastic collapse.

(i) The obtained results show a good global elastoplastic response performance of the bridge. Specifically, for the analyzed loading conditions (with vertical loads acting symmetrically with respect to the longitudinal plane of the bridge), the arch is basically never involved in the collapse mode. In this sense, it appears that the stiff doubly built-in parabolic arch, a marvellous characteristic feature of the iron bridge, represents a crucial well-set structural element, in terms of the whole global structural response of the viaduct.

(ii) Structural collapse is reached for the bridge with reference to ductile failure in the upper continuous beam and, in some cases, in some elements of the piers. Specifically, the results of Tests V–VIII have allowed to detect some possible structural deficiency referred to the upper continuous beam. When the load is discontinuously distributed on it (Figure 4), the load multipliers decrease with respect to those obtained if the same total load is considered (in terms of resultant Q) as distributed on contiguous spans (Test I and Test II). In particular,

the lowest load multipliers are obtained in the tests where the first or the last span of the beam is loaded (Test V and Test VIII). In these cases the collapse of the structure involves a large number of active modes in the beam and it is due to a collapse mechanism localized on the loaded span near the bearing bank (Figure 8). It is worth noting that the case in which the span at one end of the upper beam is loaded occurs every time a train gets on (or leaves from) the upper continuous beam. In such a case, plastic collapse is reached without showing significant plastic resources in terms of global ductility, letting this configuration to become quite critical. However, levelling results commented for *Case B* in terms of collapse load multiplier may show that the interventions on the roadway deck in the seventies and the more recent strengthening of the metallic box girder (Section 2.2), may have contributed in increasing the beam performance in terms of potential plastic collapse. Nonetheless, since the railway deck should not have undergone further substantial modifications, further checks on the structural performance of the upper continuous beam should be specifically pursued, especially considering the extremity spans supported on one side on the river banks.

(iii) Only tests with loading configurations much un-symmetrically located with respect to the crown of the arch have involved plasticity in the elements of the piers, but right underneath the loaded spans, in particular at the arch/pier and pier/beam stiffened interfaces, where the FEM model is actually not that detailed (and could be refined), to appropriately deal with the stress concentrations that may occur at these selected locations. The structural members of the arch also appear always in a rather safe position, since they are hardly involved in the plastic sequence of plastic joint activations leading to structural collapse.

(iv) The considerable level of load amplification at collapse (absolute λ_c in the order of λ_c =4.6 for Tests I–IV and in the order of λ_c =3.1–4.3 for Tests V–VIII, elastic λ_e in the order of λ_e =3.8–4.2 and multiplier ratio λ_c/λ_e in the order of 1.1, for reference *Case A*) is certainly warranted by the assumed unlimited perfectly-plastic behavior of all the structural members of the bridge, as linked to the stiff "hyperstatic" nature of the structure, as conceived at original design stage. This appears to allow for considerable stress transfer and redistribution at increasing load and resulting plastic deformation in the structure. It is worth noting that the present assumption of considering an unlimited plastic deformation ductility of the members of the bridge is consistently associated to the choice of imposing a strict yield limit of the material in the computational implementation (see discussion in Section 2.2). Moreover, the plastic deformations obtained at incipient collapse for the considered loading configurations look coherent to those expected for a structure like that of the Paderno d'Adda bridge. However, as noted again for the assumed unlimited ductility, this assumption, which may lead to possible overestimations of the collapse multipliers, is counteracted by the assumption of taking a limited value of yield strength. Thus, the present analyses, though they could be possibly further refined by considering yield mode interactions, shall be considered already representative of the main real elastoplastic performance of the structure.

(v) For particular loading configurations, the structural response of the bridge is not governed by the bending moments. Instead, it appears that, for such cases, the plasticizations related to the axial force limit the plastic resources of the structure. It means that the effect of the normal forces on the elastoplastic behavior of the bridge up to collapse is not negligible. This is confirmed also by the confrontation between the outcomes of analyzed *Cases A* and *B*.

(vi) The elastoplastic FEM formulation pointed out in this paper entails, as a present assumption, to consider an uncoupled Rankine type boxed-form yield domain in the space of the static variables. In fact, while the computing burden and inaccuracies implicit in any PWL approximation may be neglected in engineering situations such as the one treated herein, the piece-wise-linear uncoupled behavior adopted for the internal static variables may display most relevant implications. Further implementations and numerical tests considering plastic joints with interactions between the internal static variables could be considered elsewhere.

5 Conclusions

In this paper, a full structural elastoplastic analysis of the Paderno d'Adda bridge (1889) has been performed. It has been implemented within MATLAB through a dedicated computer program in which 3D beam finite elements, perfectly-plastic joints (as an extension of classical plastic hinges), piece-wise-linear yield domains and *exact* time integration have been considered as main characteristic ingredients of the elastoplastic FEM formulation.

The implemented algorithm has revealed to be very much able to track down the limit structural behavior of the bridge, by reaching convergence with smooth runs up to the true *exact* limit load and corresponding collapse displacements (i.e. collapse mechanism). This holds true despite for the considerable complexity of the complete elastoplastic bridge structure, roughly involving 5300 beam finite elements and 13300 degrees of freedom.

The elastoplastic results obtained in this paper refer to the characteristics of the bridge at design stage. They represent a first quantitative evaluation on the global elastoplastic behavior of the bridge, with an as originally conceived morphology, through the determination of the collapse multiplier and relevant collapse mechanism for various try-out loading configurations, according to the typical principles of Limit Analysis. Further, the results collected herein shall enrich the present knowledge on the structural design and performance of the Paderno d'Adda bridge. The structure was designed through the Theory of the Ellipse of Elasticity, i.e. by basically referring to considerations of elastic behavior, although supported by assuming low values of the admissible stresses in the structural elements and relying on considerable accumulated expertise on iron carpentry and local and global structural conception and care of structural details.

Final remarks on the analyses trated in this paper may be provided as follows:

- The present limit analysis shows that the bridge looks as a well-set structural system, also in the perspective of elastoplastic response and limit collapse. This appears to be reached through the considerable design knowledge achieved at the time of the design of this type of bridges and of similar co-aged truss-frame structures (see e.g. the celebrated Tour Eiffel, 1889).

- The results presented in this paper may also track down some potential critical issues of the structure, suggesting further studies on its limit structural performance, also in view of possible interventions. They should be able to address the present state of conservation of the structure, which appears to be affected by diffused and localized corrosion damage, due specifically to lack of maintenance. Ageing and corrosion may have reduced the effective cross section of the structural elements and of the plates in the joints, and led to variation of the material properties and to the presence of residual stresses, then raising current concerns on the present structural efficiency of quite a few parts of the bridge.

The following future prospective of the work may be then pointed out, also with reference to the above considerations:

- The FEM model could be further elaborated by additional information that may arise from direct detailed inspections on the bridge and from other approaches apt to handle these issues, e.g. Non-Destructive Testing, Inverse Analysis, Structural Health Monitoring and Updating of the structure and of its modelization (see e.g. Buljak et al. [17], and references quoted therein).

- Under the current loading conditions experienced by the bridge and after the extended period of 128 years of continuous duty, fatigue phenomena may arise as potentially crucial for some of the structural elements of the bridge (Pipinato and Modena [18]). Specific investigations towards the evaluation of these effects on the bridge could be further pursued.

- Extensions to second-order non-linear geometrical effects (linked to elastic or elastoplastic buckling, with a full account of the geometrical stiffness matrix or with constraints on the admissible axial stresses for the buckling of bars, see e.g. Maier [19], Kaliszky and Lógó [20],

Ferrari et al. [7]), possibly coupled to thermal effects, and to damage analyses might be considered for handling the issue of buckling as an additional limit state.

- Despite that the present modeling approach is fully deterministic, explicit strategies to consider uncertainties in conducting the limit analysis of the bridge may be considered. Uncertainties may be referred to both system parameters (e.g. material properties) and loads. A large number of computational approaches have been proposed in the literature for limit analysis of engineering structures with the considerations of various uncertain scenarios. In the classical limit analysis framework, a brief overview and a categorization of such approaches has been recently provided in Wu et al. [21]. Therein, in particular, the hybrid probabilistic interval limit analysis is introduced to assess the safety of engineering structures against plastic collapse. For considering uncertain applied loads, interesting strategies are proposed in the works by Tangaramvong et al. [22] and Kanno and Takewaki [23]. Applications of such strategies for the limit analysis of the Paderno d'Adda bridge might be the goals of forthcoming research scenarios.

References

[1] Società Nazionale delle Officine di Savigliano (1889). Viadotto di Paderno sull'Adda (Ferrovia Ponte S. Pietro-Seregno). Torino: Tip. e Lit. Camilla e Bertolero.

[2] Nascè, V., Zorgno, A.M., Bertolini, C., Carbone, V.I., Pistone, G., Roccati, R. (1984). Il ponte di Paderno: storia e struttura - Conservazione dell'architettura in ferro. *Restauro*, Anno XIII, n. 73–74, 215 pages.

[3] Ferrari, R., Rizzi, E. (2008). On the theory of the ellipse of elasticity as a natural discretisation method in the design of Paderno d'Adda Bridge (Italy). *6th Int. Conf. on Structural Analysis of Historical Construction (SAHC08)*, Bath, UK, 2-4 July 2008, Vol. 1, pp. 583–591.

[4] Ferrari, R., Facheris, M., Rizzi, E. (2010). Structural analysis of the Paderno d'Adda Bridge (Italy, 1889). *7th Int. Conference on Structural Analysis of Historical Constructions (SAHC10)*, Shanghai, China, 6-8 October 2010, Advanced Materials Research, Vols. 133–134 (2010), 459–465.

[5] Ferrari, R., Rizzi, E. (2011). FEM modelling of the Paderno d'Adda bridge (Italy, 1889). In *Proc. of Structural Engineers World Congress (SEWC 2011)*, Como, Italy, 4-6 April 2011, Book of Abstracts p. 159; CD-ROM Proceedings, Paper 210, 9 pages.

[6] Ferrari, R., Cocchetti, G., Rizzi, E. (2012). Elastoplastic Structural Analysis of the Paderno d'Adda bridge (Italy, 1889) based on Limit Analysis. *8th Int. Conf. on Structural Analysis of Historical Constructions (SAHC2012)*, Ed. Jerzy Jasieńko, Wroclaw, Poland, October 15-17, 2012, Vol. 3, pp. 2171–2180. Also selected to appear in Wiadomości Konserwatorskie – Journal of Heritage Conservation, Stowarzyszenie Konserwatorów Zabytków – Association of Monument Conservators, Poland, Nr. 34/2013, p. 28-35.

[7] Ferrari, R., Cocchetti, G., Rizzi, E. (2016). Limit Analysis of a historical iron arch bridge. Formulation and computational implementation. *Computers & Structures*, to appear on line, DOI: 10.1016/j.compstruc.2016.05.007.

[8] Gentile, C., Saisi, A. (2010). Dynamic assessment of the iron bridge at Paderno d'Adda (1889). *7th Int. Conference on Structural Analysis of Historical Constructions (SAHC10)*, Shanghai, China, 6-8 October 2010, Advanced Materials Research, Vols. 133–134 (2010), 709–714.

[9] Gentile, C., Saisi, A. (2011). Ambient vibration testing and condition assessment of the Paderno iron arch bridge (1889). *Construction and Building Materials*, 25(9): 3709–3720.

[10] Maier, G. (1970). A matrix structural theory of piecewise-linear plasticity with interacting yield planes. *Meccanica*, 5(1): 54–66.

[11] Maier, G. (1976). Piecewise linearization of yield criteria in structural plasticity. *Solid Mechanics Archives*, 1(2/3): 239–281.

[12] Capurso, M. (1971). Limit analysis of continuous media with piecewise linear yield condition. *Meccanica*, 6(1): 53–58.

[13] Hodge Jr., P.G. (1977). Automatic piecewise linearization in ideal plasticity. *Computer Methods in Applied Mechanics and Engineering*, 10(3): 249–272.

[14] Tin-Loi, F. (1990). A yield surface linearization procedure in limit analysis. *Mechanical Structures and Machines*, 18(1): 135–149.

[15] Olsen, P.C. (1998). The influence of the linearization of the yield surface on the load-bearing capacity of reinforced concrete slabs. *Computer Methods in Applied Mechanics and Engineering*, 162(1-4): 351–358.

[16] Jiràsek, M., Bažant, Z.P. (2002). Inelastic Analysis of Structures. Chichester, UK: Wiley.

[17] Buljak, V., Cocchetti, G., Cornaggia, A., Garbowski, T., Maier, M., Novati, G. (2015). Materials Mechanical Characterizations and Structural Diagnoses by Inverse Analyses. Chapter 20. Handbook of Damage Mechanics, G.Z. Voyiadjis (ed.), Springer Science+Business Media, New York, 2015.

[18] Pipinato, A., Modena, C. (2010). Structural analysis and fatigue reliability assessment of the Paderno bridge. *Practice Periodical on Structural Design and Construction*, ASCE, May 2010/109: Vol. 15, No. 2, pp. 109–124.

[19] Maier, G. (1971). Incremental plastic analysis in the presence of large displacements and physical instabilizing effects. *International Journal of Solids and Structures*, 7(4): 345–372.

[20] Kaliszky, S., Lógó, J. (2002). Plastic behaviour and stability constraints in the shakedown analysis and optimal design of trusses. *Structural and Multidisciplinary Optimization*, 24(2): 118–124.

[21] Wu, D., Gao, W., Tin-Loi, F., Pi, Y.-L. (2016). Probabilistic interval limit analysis for structures with hybrid uncertainty. *Engineering Structures*, 114(2016): 195–208.

[22] Tangaramvong, S., Tin-Loi, F., Wu, D., Gao, W. (2007). Mathematical programming approaches for obtaining sharp collapse load bounds in interval limit analysis. *Computers & Structures*, 125(2013): 114–126.

[23] Kanno, Y., Takewaki, I. (2007). Worst case plastic limit analysis of trusses under uncertain loads via mixed 0-1 programming. *Journal of Mechanics of Materials and Structures*, 2(2): 245–273.